THE DISTRIBUTION OF DOSE AND INDUCED ACTIVITY AROUND EXTERNAL PROTON BEAM TARGETS

G S Levine*), Dorothea M Squier, G B Stapleton, G R Stevenson
Rutherford High Energy Laboratory, United Kingdom

K Goebel
European Organisation for Nuclear Research (CERN)

J Ranft
Karl Marx Universität, Leipzig, DDR

1 INTRODUCTION

One of the many problems involved in planning a particle accelerator facility is the prediction of the effects of stray radiation arising from beam loss. Amongst these effects are the radioactivity induced in magnets and other parts of the accelerator structure and degradation of magnet insulation and of other components susceptible to radiation damage. These are factors which will influence efficient operation and management of the accelerator. For example, radiation sensitive components may require frequent replacement, but high dose rates from induced radioactivity impose restrictions on access for maintenance. In order to calculate the magnitude of these effects, one must be able to predict dose rates and hadron flux densities as a function of position around points of known beam loss. Essential to such predictions (using Monte Carlo transport calculations, for example) is a knowledge of the angular distribution of the secondary particles produced in proton-nucleus collisions.

Measurements of momentum-integrated secondary particle yields have been made around internal targets[1-3], but because of uncertainties in the number of protons interacting in the target and ill-defined source geometry the results were difficult to interpret in terms of the proton-nucleus interaction. Some proton-nucleus yield data have been obtained at 3GeV using an external target[4], but available data at high energies (7GeV, Ref. 5) are of limited accuracy. There is a large amount of data on individual hadron yields from proton-proton and proton-nucleus

---

* normal address: Brookhaven National Laboratory, Upton, L.I. New York 11973, U.S.A.

interactions at small angles (see the Bibliography of Ref. 6). The data which exist for large angle secondary particle production from proton-proton collisions are inadequate for calculation of the large angle yield from poorly developed cascades in materials of high atomic weight.

More extensive data were required to provide an adequate basis for the Monte Carlo and other transport model calculations for the projected 300GeV accelerator. The validity of these models must be checked against such data, but the data themselves are also useful for simple extrapolation to energies where no theoretical models are available, and when similar experimental conditions are expected in a new situation. It was decided to carry out experiments to obtain the momentum integrated hadron yields at different proton energies and with different target materials.

2 EXPERIMENTAL PROCEDURE

2.1 Targets

Target dimensions of 2cm diameter x 5cm length were chosen for these experiments. The diameter is large enough to ensure that a typical extracted beam, incident along the cylindrical axis, continues to interact within the target despite the usual slight variations in steering, without significantly modifying the high energy radiation emitted at wide angles. The choice of length also represents a compromise between an adequate number of primary interactions and minimal development of the extra-nuclear cascade.

Details of the target irradiations are given in Table 1. Because of the limited machine time available, it was decided to study the dependence of yields on primary energy using only a copper target, and to investigate variations with target nucleus at the lower available energy.

Table 1

Target irradiation conditions

Beam	Momentum (GeV/c)	Target	Beam Intensity[a] (protons/sec)	Duration (mins)
CERN P.S. e7	24	Cu	3.06×10^{11}	281
NIMROD X3	8	Cu	1.50×10^{11}	315
NIMROD X3	8	"Heavy alloy"[b]	7.18×10^{10}	91
NIMROD X3	8	Al	2.33×10^{11}	260
NIMROD X3	8	none[c]	2.24×10^{11}	244

a) Measured using the reaction $^{27}Al(p,3pn)^{24}Na$. Assumed cross section = 8.6 mbarns at 8GeV/c and 24GeV/c.

b) "Heavy alloy" is a trade name of G.E.C. Ltd. The alloy contains 90%W, 7.5%Ni and 2.5%Cu by weight.

c) The experiment with no target was included to check on the effects of interactions of the proton beam with the sample array itself.

The beam cross-section at the target was in each case smaller than 3mm x 5mm. Care was taken to ensure that the beam passed along the axis of each target.

2.2 Dose and fluence measurements

The sample array for each irradiation was built up on a baseboard of expanded polystyrene. Plans of the baseboards used in the experiments at the two accelerators are shown in Figure 1. 10cm wide strips of aluminium (500μm thick), polytetrafluoroethylene (250μm thick) and polyethylene (1mm thick) were mounted on the baseboard in arcs of specified radii around the target. Hydrogen pressure, thermoluminescent and $\beta - \gamma$ film dosimeters and some larger discrete samples of aluminium, suplphur, gold, PTFE and plastic scintillator were secured in selected positions on the arcs (see Figure 1). After the irradiations, discs of a size appropriate to their position in the arrays were punched out of the strips and activity measurements made on these discs. This technique of sample location made it possible to determine accurately

the position of each sample relative to the baseboard and thus relative to the target.

For the analysis described in this paper, we are concerned only with the following detection techniques:- Hydrogen pressure dosimeters (HPD), ^{7}LiF thermoluminescent dosimeters (TLD), and the activity measurements of ^{7}Be in polythene and ^{18}F in aluminium. A complete description of all the measurements is to be published elsewhere.

2.3 Description of the experimental techniques

2.3.1 RHEL Hydrogen pressure dosimeters

Irradiated polyethylene releases hydrogen gas as a result of radiation induced molecular disruption. The dosimeter designed at RHEL for megarad dosimetry[7)] has a 1.5g cylinder of polyethylene placed in a small evacuated glass capsule. After irradiation the capsule is broken in an evacuated container of known volume and the pressure measured in this container. From this the mass of gas released from the polyethylene can be calculated.

The useful range of this dosimeter extends from 10^{4} - 10^{9} rads. Calibration was carried out against standard Fricke-type dosimeters in a spent reactor fuel element facility.

2.3.2 ^{7}LiF thermoluminescent dosimeters

The Harshaw TLD-700 used was obtained from the Radiological Protection Service, Belmont, Surrey, U.K. Each dosimeter consisted of 30mg of powder contained in a PVC self-adhesive sachet. After irradiation the dosimeters were returned to the RPS for measurement. The useful dose range is from 10^{-2} - 10^{5} rads and calibration was effected using filtered ^{226}Ra γ radiation.

2.3.3. ^{7}Be in polythene

The ^{7}Be induced in the polyethylene of the hydrogen pressure dosimeters by the reaction ^{12}C(x,x2p3n)^{7}Be was measured after the dosimeters had been broken for dose assessment. The activity was assayed by gamma spectrometry with a NaI(Tl) scintillator. (^{7}Be has a 53 day half-life and decays by electron capture, 10% of the decays resulting in the emission of a photon having an energy of 0.477MeV).

A production cross-section of 11 mbarns was assumed: flux densities calculated from this correspond to those of hadrons having energies greater than 40MeV.

2.3.4 ^{18}F in aluminium

Spallation reactions in aluminium lead to the formation of ^{18}F, which has a half-life of 1.83 hours, emitting positrons of 0.635MeV max. ^{18}F was assayed by gamma spectrometry as above, but in this case the measurement of the 0.511MeV annihilation quanta is complicated by the presence of the 1.369 and 2.754MeV gamma rays from ^{24}Na. The procedure adopted was to make at least three measurements of each sample, which permitted accurate subtraction of the counts included in the 0.511MeV window from the Compton continuum of the higher energy γ rays of ^{24}Na. A production cross-section of 8 mbarns was assumed: flux densities again correspond to those of hadrons having energies greater than 40MeV.

3 RESULTS

All dose and fluence results obtained at different radii show a departure from a pure inverse square distance dependence (see Figure 2). At small radii this arises from the finite length of the target, while at larger radii the emitted particles undergo further interactions with the material of the experimental array itself.

Despite these limitations, in order to compare all the experimental data directly the results were normalised to a radius of 1 metre using a pure inverse square relation. The spread between data points at the same angle but different radii, reflecting departure from $1/r^2$, is only of the same order of magnitude as the measurement uncertainties (ie counting statistics or differences in dosimeter response in this radiation environment): the data taken at 24GeV/c also suffer from errors of position at low angles, due to a small movement of the array during the irradiation.

4 COMPARISON OF MEASUREMENTS WITH THEORETICAL PREDICTIONS

Two theoretical approaches have been used to give the integrated momentum spectra of secondary particles from proton-proton collisions as a function of angle, namely the thermodynamical model (see for

example Refs. 8 and 9) and a modification of the semi-empirical Trilling formula [10]). A comparison of the predictions for 24GeV/c protons in terms of the angular dependence of hadron yields (ie integrated momentum distributions), given in Figure 3, shows agreement between the two methods within the statistical accuracy of the calculations. The thermodynamical model is a more fundamental representation of the proton-proton interaction, while the modified Trilling formula is simpler to use in Monte Carlo calculations of the extranuclear cascade.

Dose and hadron flux distributions normalised to 1 metre radius are shown in Figures 4 and 5 (24GeV/c data) and Figures 6 and 7 (8GeV/c data). In Figure 4, differences between results from the two dosimeter types at wider angles arise both from a systematic difference in response and from the inaccuracy of measurements near the dose threshold of the Hydrogen pressure dosimeters. There is reasonable agreement between the experimental data and the predictions of the modified Trilling formula at angles $< 30^{\circ}$. Measurements of the hadron yield with the two activation detector techniques show good mutual agreement over a wide range of angles, and also agree with the theoretical predictions below 30° (see Figure 5).

Measurements at 8GeV/c were carried out over a wider range of angles. The dose distribution shown in Figure 6 contains results from a smaller number of individual dosimeters; the discontinuity between 45° and 60° again reflects the inaccuracy of measurements near the threshold of the HPD and the upper dose limit of the TLD. As before, good agreement with predictions at small angles is evident. In addition, the hadron flux data show good agreement with predictions at small angles (Figure 7), and are also self-consistent over a wide range of angles.

There is therefore good agreement on an absolute basis between our experimental data and calculations based on single proton-proton interactions for dose and hadron flux distributions at angles smaller than 30°. Divergence from predictions is expected at larger angles due to the particles produced with significant transverse momenta in the intranuclear cascade of proton-nucleus interactions. Data obtained with different target materials (Al, Cu and W) will indicate the dependence of the magnitude of this component on the atomic weight of

the nucleus. Nuclear evaporation also gives rise to a significant transverse component, but the target was large enough to absorb charged evaporation particles, which would contribute to measured dose, while the energy threshold in the hadron flux measurements was too high for the detection of significant numbers of particles from this process.

5 PRACTICAL APPLICATIONS

Because of the agreement below 30°, ie for the particles which control the development of the cascade, we have more confidence in the results of extranuclear cascade calculations[11], which are based on the theoretical proton-proton interaction data used for this paper. Results of particular interest from these calculations include both energy deposition and star density. The calculated energy deposition is directly related to absorbed dose measured as rads in tissue. The HPDs are calibrated to measure rads in polyethylene which can be taken to be equivalent to tissue. So it is possible to assess the dose to a person accidentally exposed in a high beam loss area either by calculation or by extrapolation from the existing HPD data.

In a similar fashion it is possible either to calculate or to extrapolate values for the absorbed dose in an insulator or other sensitive structure. It should be borne in mind that the HPD will give a better estimate of absorbed dose in an organic material while the TLD, containing no hydrogen, should give the dose in a low atomic weight, inorganic material.

In an equilibrium hadron cascade the spatial distribution of radioactive nuclei produced by spallation is expected to be similar to that of the calculated star density. Thus the calculated hadron cascade star densities should be proportional to the γ dose rate resulting from the decay of these nuclei. The constant of proportionality has been determined for cascades in iron and used to predict dose rates from remanent activity which are in accord with practical experience[12].

6 ENERGY SCALING AT LARGE ANGLES

Comparison of the hadron flux distributions at 8GeV/c and 24GeV/c, shown in Figure 8, indicates no detectable increase of yield

with energy over the angular range 30^{o} - 80^{o}. Energy independence of the yield at large angles in hadron-hadron collisions is predicted by the thermodynamic model which, in common with other current models of hadron production, demonstrates the hypothesis of limiting fragmentation[13]. This hypothesis asserts that at large angles the momentum distribution of secondary particles approaches a limiting condition with increasing incident energy, thus the momentum-integrated angular distributions become independent of primary energy.

The secondary particle yields at large angles from hadron-nucleus interactions are considerably enhanced by contributions from the intranuclear cascade and nuclear evaporation. Our data indicate that there is no scaling with energy of the large angle yields from the combined effects of proton-proton collisions and the intranuclear cascade.

7 IMPLICATIONS FOR HIGHER ENERGY ACCELERATORS

When the beam hits an extended beam stop in a tunnel the hadronic cascade develops in the beam stop, and the transverse shielding required for the tunnel can be determined from cascade transport calculations which are in good agreement with experimental data[14]. This procedure fails in the case of a thin target which does not allow significant development of the cascade. Until reliable particle production formulae for large angle production in hadron-hadron collisions become available, it will be impossible to carry out transport calculations to indicate shielding requirements at 90^{o} for a thin target. The hypothesis of limiting fragmentation, however, would imply that the transverse shielding requirements in this situation should be the same at 300GeV as at 20 - 30GeV.

The remanent radioactivity in iron shielding at right angles to a thin target at 300GeV should also be directly calculable from data at presently available proton energies. The activation of concrete may well be similar at 300GeV and present energies, but since the thermal neutron component of the field is more important in this case than in the activation of iron, remanent dose rates will be rather more dependent on local conditions.

8 ACKNOWLEDGEMENTS

The work described in this paper formed part of studies for the 300GeV Radiation Problems Group.

The authors acknowledge the assistance of Dr J H Madsen (CERN, M P S Division) and Mr R G Russell (RHEL, Nimrod Division) and their operating crews in providing the necessary machine time.

We thank Dr J Baarli (Health Physics) and Dr C D Johnson (M P S) for laboratory facilities provided at CERN, and members of the Radiation Protection and Chemical Technology Groups at RHEL for their generous assistance during the experiments.

* * *

REFERENCES

1) S Charalambus, K Goebel and D Nachtigall, CERN DI/HP/97 (1967)

2) W S Gilbert et al, UCRL-17941 (1968)

3) C D Johnson, R Sheldon and G B Stapleton, RHEL/M 175 (1969)

4) M Awschalom and W Schimmerling, PPAD 655E (1969)

5) G R Stevenson et al, RHEL/M 148 (1969)

6) J Ranft, Physics Letters, 31B, 529 (1970)

7) A Morris, R Sheldon and G B Stapleton, RHEL/R 132 (1966)

8) R Hagedorn and J Ranft, Suppl. Nuovo Cimento, 6, 196 (1968)

9) R Hagedorn, Astron. and Astrophys., 5, 184 (1970)

10) J Ranft, Nucl. Inst. and Methods, 48, 133 and 261 (1967)

11) J Ranft and E Freytag, to be published

12) K Goebel, J Ranft and G R Stevenson, to be published

13) J Ranft, TUL 43 (1971)

14) K Goebel and J Ranft, CERN 70-16 (1970)

FIGURE CAPTIONS

Figure 1 Sample rigs for target yield experiments

Figure 2 Variation of dose with radial distance (24GeV/c)

Figure 3 Comparison of hadron fluxes predicted by theoretical models

Figure 4 Comparison of predicted and measured dose (24GeV/c)

Figure 5 Comparison of predicted and measured hadron flux density (24GeV/c)

Figure 6 Comparison of predicted and measured dose (8GeV/c)

Figure 7 Comparison of predicted and measured hadron flux density (8GeV/c)

Figure 8 Comparison of hadron flux densities measured at 8GeV/c and 24GeV/c

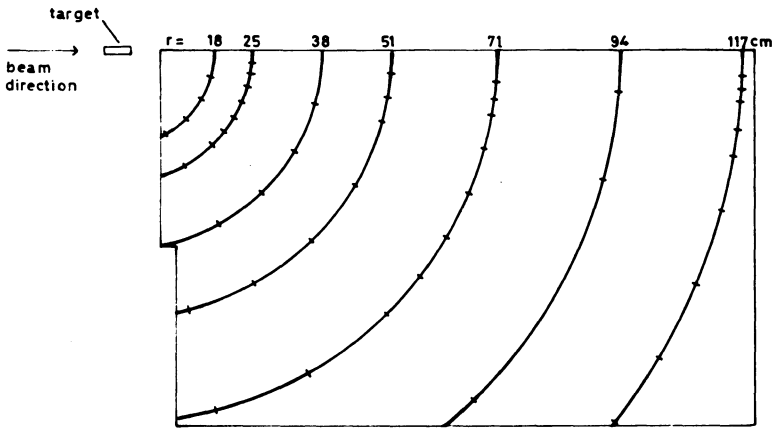

(i) CERN P.S. sample rig
(mounted vertically)

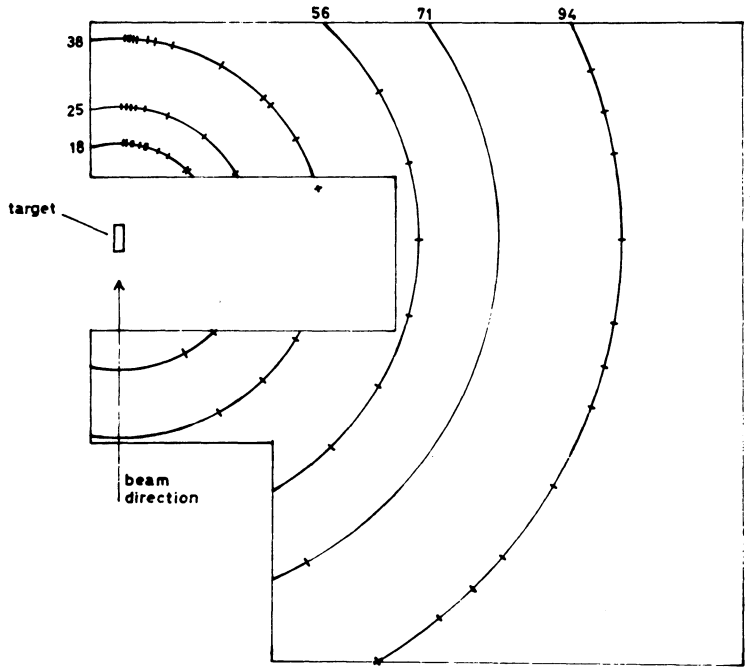

(ii) RHEL Nimrod sample rig
(mounted horizontally)

Figure 1. Sample rigs for target yield experiments

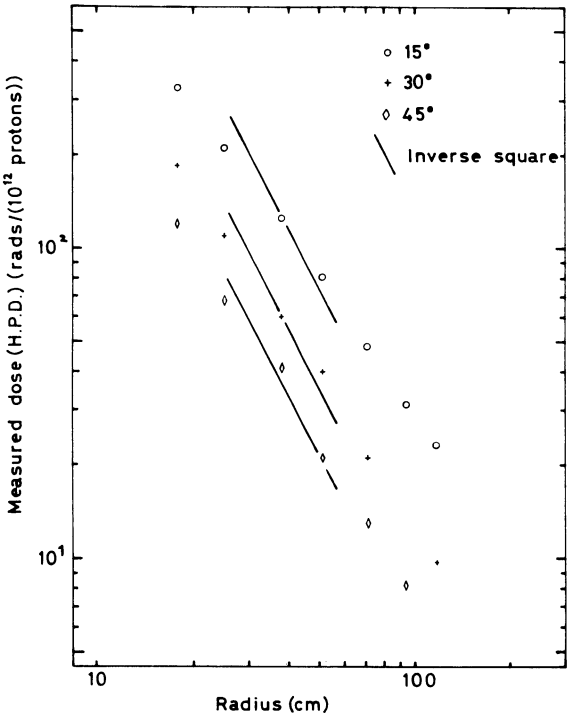

Figure 2. Variation of dose with radial distance (24 GeV/c)

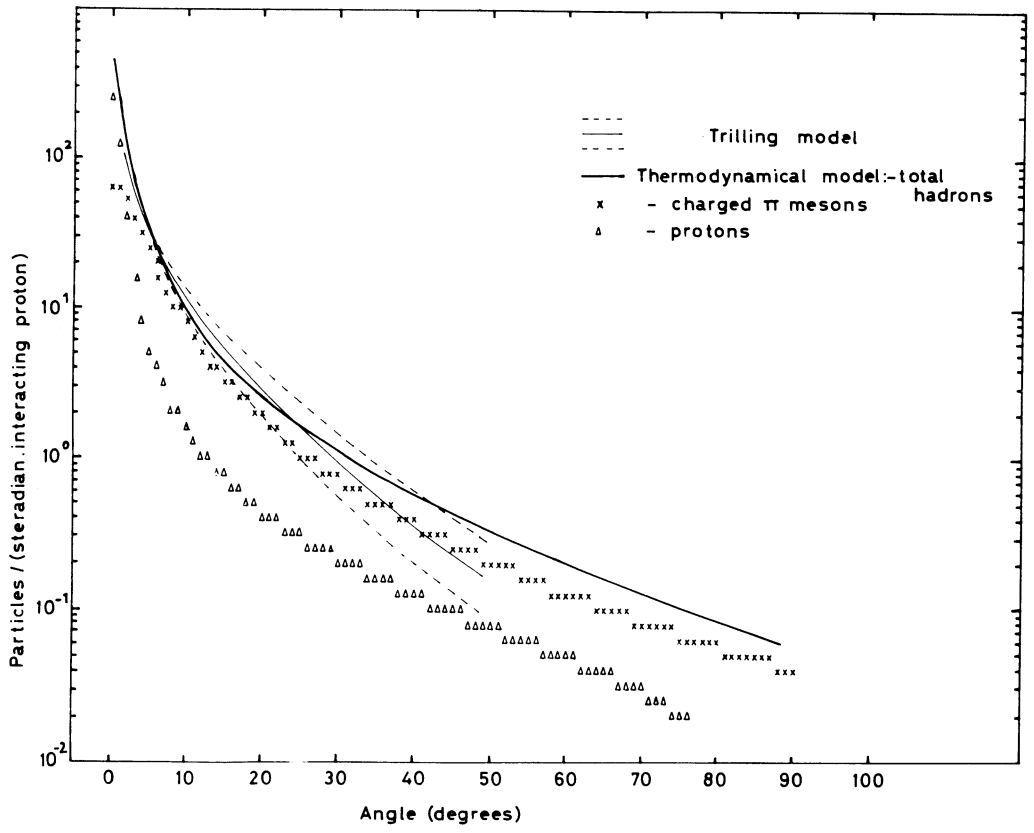

Figure 3. Comparison of hadron fluxes predicted by theoretical models (24 GeV/c)

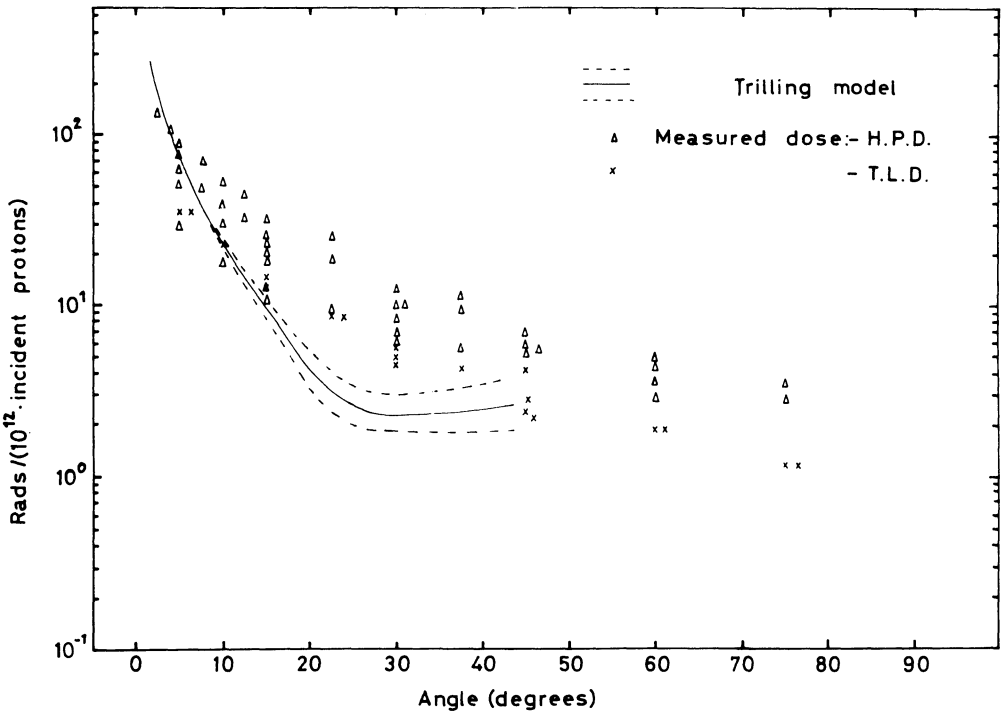

Figure 4. Comparison of predicted and measured dose (24 GeV/c)

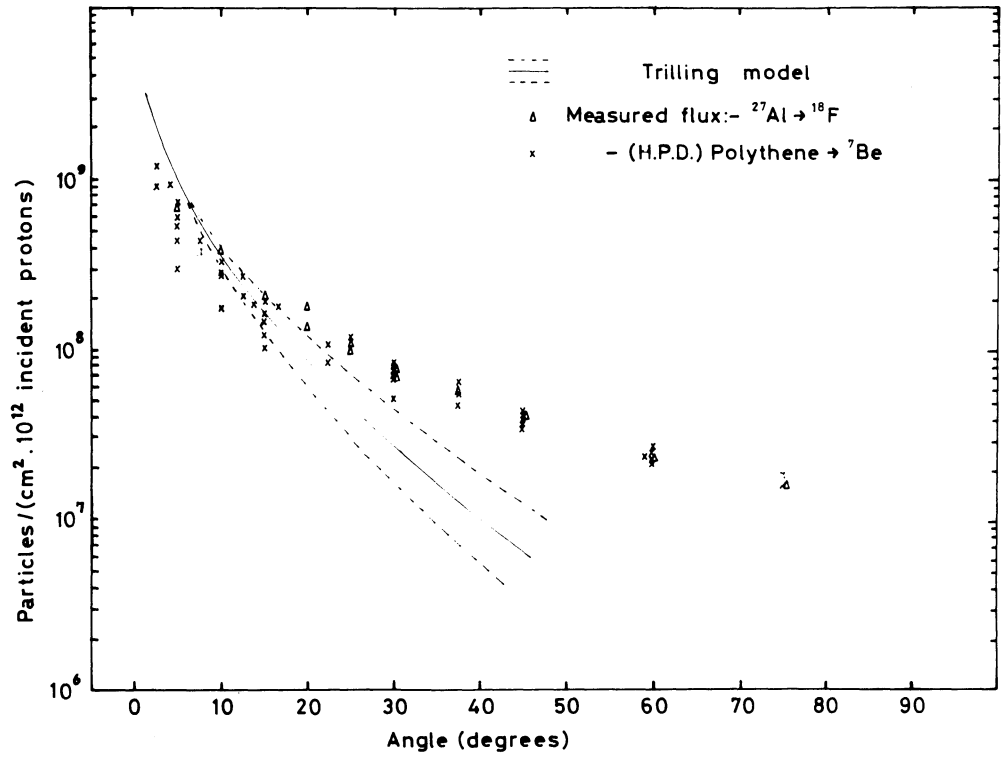

Figure 5. Comparison of predicted and measured hadron flux density (24 GeV/c)

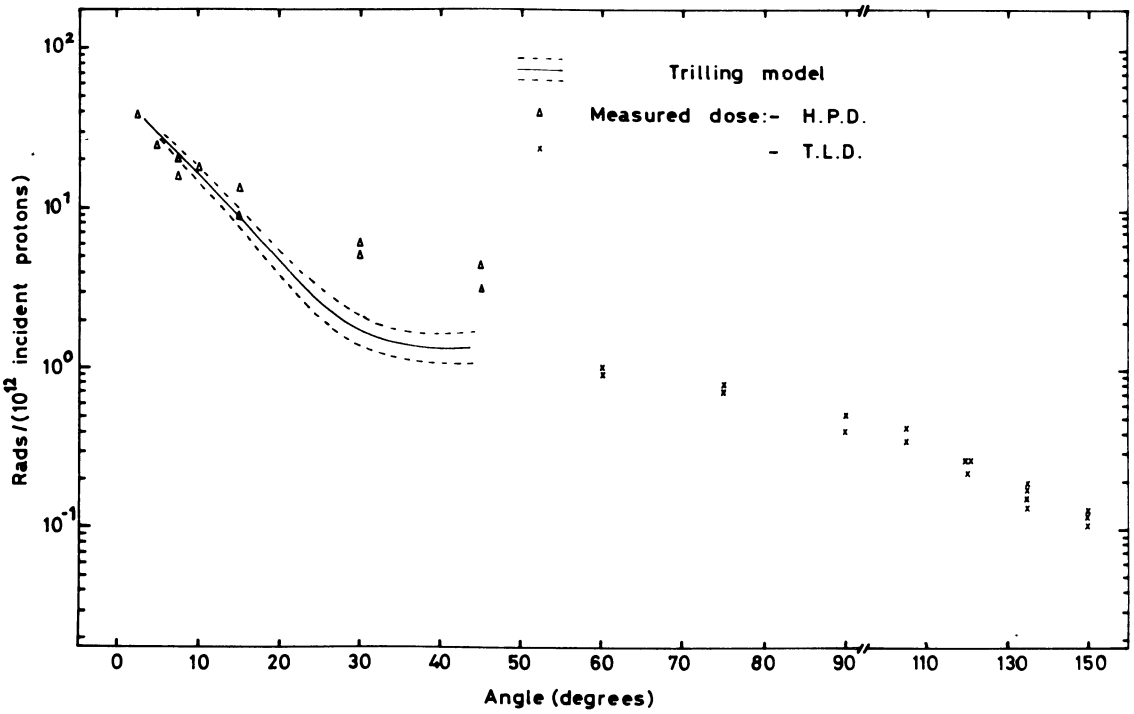

Figure 6. Comparison of predicted and measured dose (8 GeV/c)

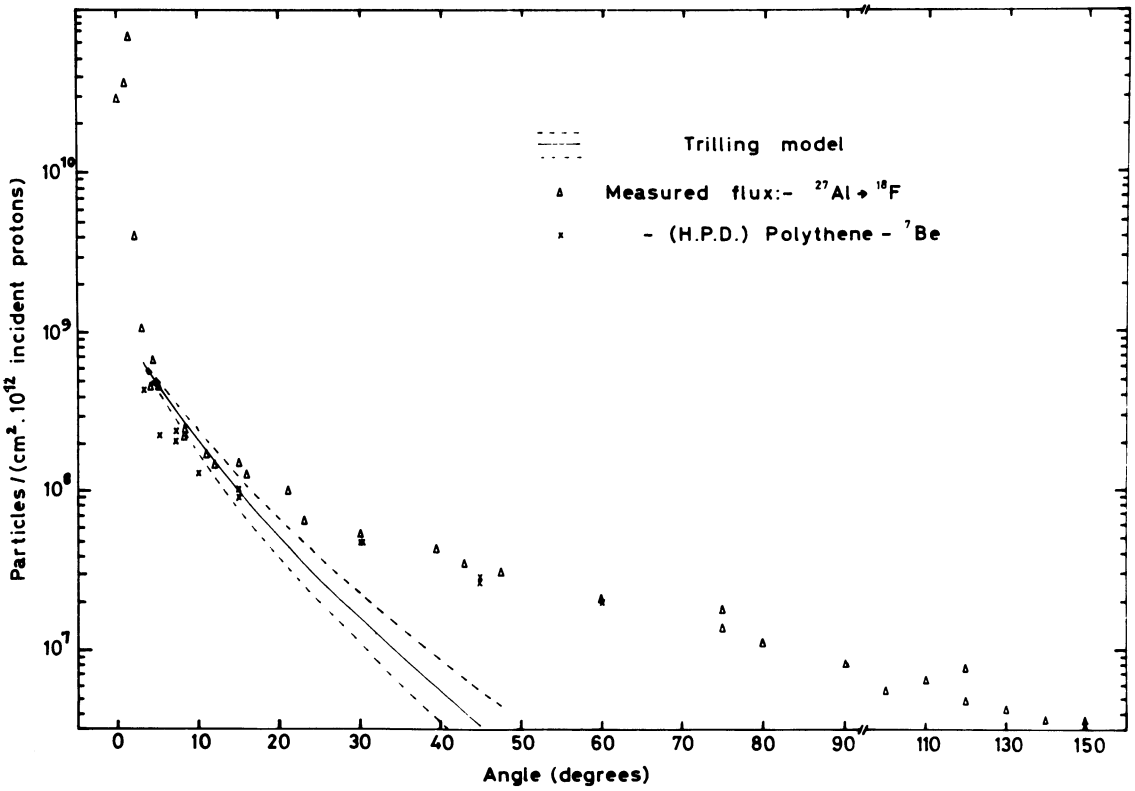

Figure 7. Comparison of predicted and measured hadron flux density (8 GeV/c)

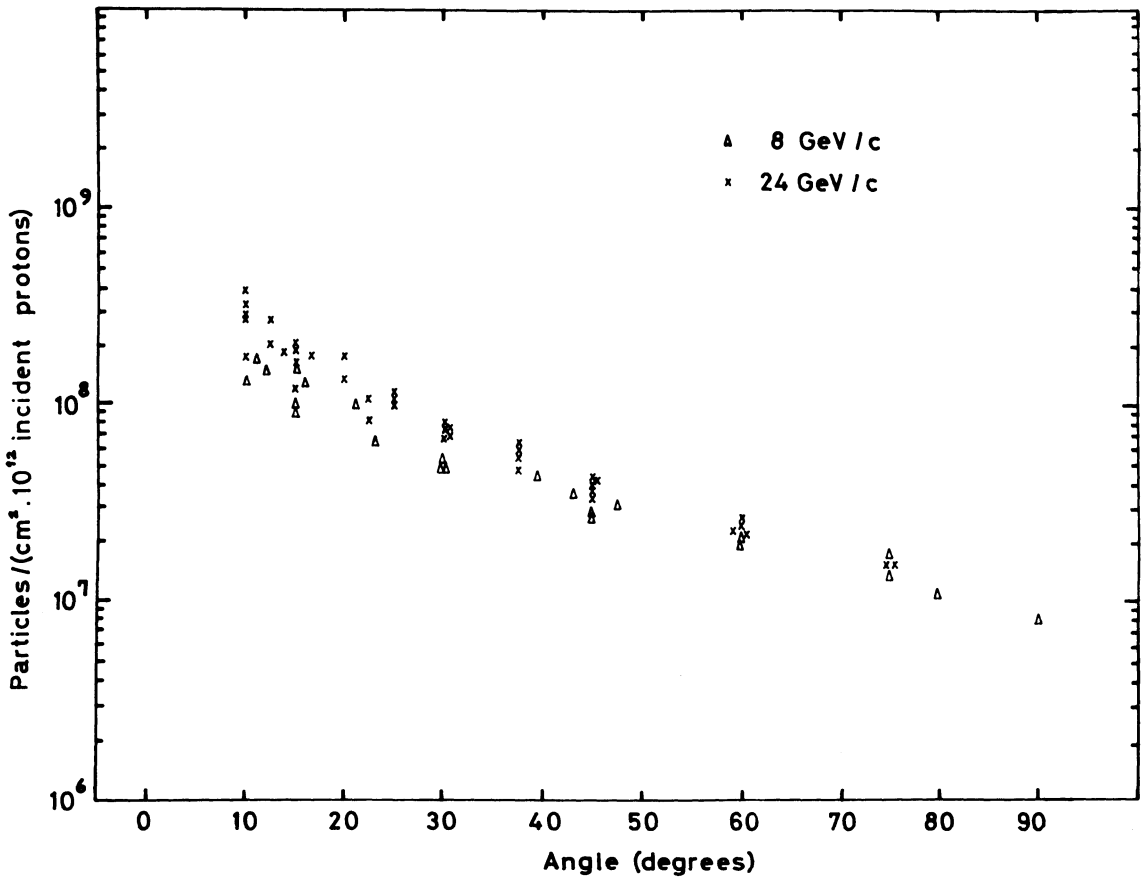

Figure 8. Comparison of hadron flux densities measured at 8 GeV/c and 24 GeV/c.

DISCUSSION

Paper : The distribution of dose, and induced activity around external proton beam targets

AWSCHALOM: In Fig. 8, the graphs show flux per incident proton. Do you mean incident or interacting?

STEVENSON: I referred to incident protons since at both energies the target was of identical dimensions and material, viz. 2 cm ϕ × 5 cm long, copper.

GOLLON: How does dose-rate at large angles ($\sim 90^\circ$) scale with incident proton energy?

STEVENSON: Dose for incident proton increases by about a factor of two for an increase in proton momentum from 8 GeV/c to 29 GeV/c. All high-energy hadron detector systems gave practically no increase in fluence for proton with proton energy -- an increase was only detectable with the lower energy neutron detectors, for exemple, ^{24}Na from ^{27}Al.

ROUTTI: The prediction based on the Ranft-Trilling formula is obtained by integrating over momentum, I assume. What integration limits were used to obtain the dose, and did you integrate directly or through Monte-Carlo procedures? How is the increase of dose above 30° possible, as indicated by the prediction in one of your slides?

RANFT: The curves were obtained by a Monte-Carlo procedure in which doses and star densities were calculated also in the material downstream of the detectors. Only particles with energies higher than 50 to 100 MeV are considered in the Monte-Carlo calculation. One of the curves given shows signs of statistical errors near 30°. Figure 3 of the paper gives curves which are obtained by integrating the thermodynamic particle spectra over momentum. These curves agree approximately with the Monte-Carlo results of the angular dependence of particle fluxes.